IEEE Photonics Journal
An IEEE Photonics Society Publication

Design of a Single-Lens Freeform-Prism-Based Distortion-Free Stereovision System

Volume 11, Number 4, August 2019

Xiaoyu Cui
Liqian Wang
Yuetian Ren
Shuo Chen
Yue Zhao
Kahbin Lim
Tianxing Gong

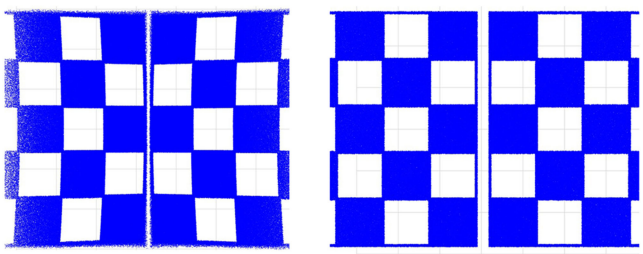

DOI: 10.1109/JPHOT.2019.2924458

IEEE photonics SOCIETY
IEEE

Design of a Single-Lens Freeform-Prism-Based Distortion-Free Stereovision System

Xiaoyu Cui,[1,3] Liqian Wang,[1] Yuetian Ren,[1] Shuo Chen,[1,3] Yue Zhao,[1] Kahbin Lim,[2] and Tianxing Gong[1]

[1]School of Sino-Dutch Biomedical and Information Engineering, Northeastern University, Shenyang 110819, China
[2]Department of Mechanical Engineering, National University of Singapore, Singapore 119077
[3]Key Laboratory of Data Analytics and Optimization for Smart Industry, Northeastern University, Shenyang 110819, China

DOI:10.1109/JPHOT.2019.2924458

Manuscript received May 9, 2019; accepted June 19, 2019. Date of publication June 24, 2019; date of current version July 10, 2019. This work was supported in part by the National Natural Science Foundation of China under Grants 61501101, 61605025 and 71621061, in part by the 111 Project (B16009), and in part by the Fundamental Research Funds for the Central Universities under Grants N171904006, N171902001, and N172410006-2. Corresponding author: Shuo Chen (e-mail: chenshuo@bmie.neu.edu.cn).

Abstract: Stereo vision can be achieved with a single camera aided by a flat-face prism. However, large optical distortions may be caused by irregular refraction. To mitigate this deficiency and minimize distortion, a new freeform prism design is proposed to replace the flat-face prism. All refracting surfaces of the prism are designed for freeform features, which can process object points at a large depth of field. Differential equations are derived to express the freeform surface, and the Runge–Kutta method is used to numerically solve the differential equations.

Index Terms: Optical imaging techniques, image distortion, image rectification.

1. Introduction

The single-lens prism-based stereovision (PbS) system can reconstruct a 3D scene. Such a system, which uses only one camera, significantly simplifies the integration effort of a stereovision system. In the past few years, this type of system has been applied to many fields such as medical endoscopes [1], [2], microscopic measurement [3], deformation measurement [4], velocity measurement [5] and occlusion detection [6].

The PbS system was first proposed by Lee *et al.* in 2000 [7]. In their study, a biprism was used to symmetrically transform an object point in 3D space into two virtual points, whose separation distance was proportional to the depth of the object point. However, this model did not consider the nonlinear distortion caused by the biprism, which limited the shape retrieval accuracy. Thereafter, in their pioneering work, by placing a prism in front of a camera lens, Lim *et al.* [8] introduced a method, which assumed that a scene captured by a PbS system would give rise to two images captured by two virtual camera systems [8], [9]. This work enables the application of conventional stereovision modeling methods and analyses such as calibration [10] and stereo correspondence matching [11]. Then, extended methods such as multiprism [12] and microprism array [13] were

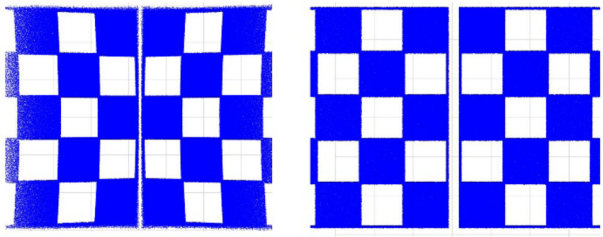

Fig. 1. Simulation results of the realistic checkerboard image using Zemax. (a) Image captured by the Pbs system with a flat surface. (b) Image captured by the Pbs system with a freeform surface, which is designed by our proposed method.

proposed. In our previous studies, the prism was considered a single optical device, and a virtual point model was proposed to depict the relationship between an object point and its image points [14]. Based on this study, we developed a method to estimate the position of the prism [15] and a perspective projection model to express the homography between an object and its image [16]. Wu *et al.* modified the virtual point model and proposed a bilateral telecentric lens-based PbS system [17]; they also developed a practical shape retrieval method [18], which could further improve the shape retrieval accuracy of this technique.

Although a regular prism with flat surfaces can be used to form stereo images, it will induce additional unique distortion in the image, which cannot be adequately represented by the existing distortion models, as shown in Fig. 1(a). To solve this problem, many image-based [19] or optical-based [3], [20], [21] methods were proposed by researchers. [19] developed a parametric biprism distortion model to correct this type of distortion; [20] introduced a rectifying method by adding another auxiliary camera; [21] used a concave mirror for discrepancy compensation; and [3] designed a freeform prism array, which can reduce the image distortion.

In this paper, we propose a novel method in the design of freeform prisms to minimize the image distortion caused by a traditional flat-face prism (Fig. 1(b)). This work has three main contributions. First, we present a modified virtual camera model as a basis to correct the refractive ray of the flat prism, which can be widely used for stereovision applications. Second, we develop a new design methodology of a prism with freeform features for the slanted refracting surfaces, which can improve the spatial resolution of depth. Third, we derive a pair of differential equations to describe the freeform surfaces with a numerical solution algorithm using the Runge-Kutta method. We believe that our proposed freeform PbS system can acquire undistorted stereo image pairs at a single shot of the camera, and we directly implement the stereo correspondence algorithm without image rectification.

2. Method

In a PbS system, a prism is placed in front of a single camera to split its field of view and generate image pairs of the target. These image pairs can be considered as being captured by virtual cameras from different viewpoints [9]. It is assumed that each virtual camera consists of one unique optical center and a planar image plane, which are determined by two boundary rays, as shown in Fig. 2(a). However, other refracted rays emitted from the image plane cannot converge exactly at the optical center [3], [19]–[21]. Thus, the hypothetical virtual cameras cannot accurately obey the pinhole camera model, which will induce additional distortion in the image. Moreover, although this type of distortion can be corrected by some image-based methods [19], the virtual horizontal image planes do not aligned, which implies that the epipolar line rectification must also be implemented for subsequent processing. In contrast, by replacing the flat surface of the prism with a freeform surface, we construct a modified virtual camera model, with which the virtual cameras will satisfy the requirements of the pinhole camera model and the standard epipolar geometry, as shown in

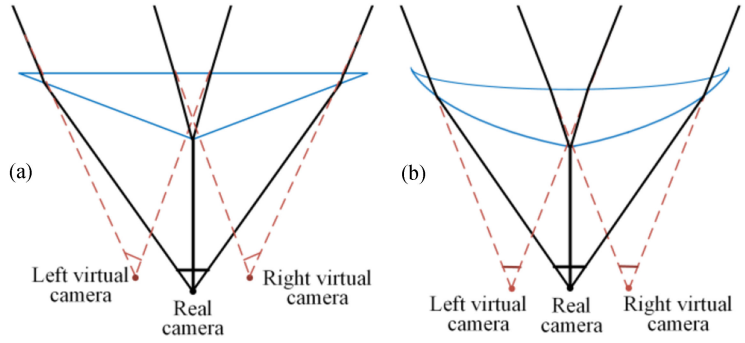

Fig. 2. Virtual camera model. (a) Virtual camera model of the flat-prism-based stereovision system. (b) Modified pinhole virtual camera model of the freeform-prism-based stereovision system.

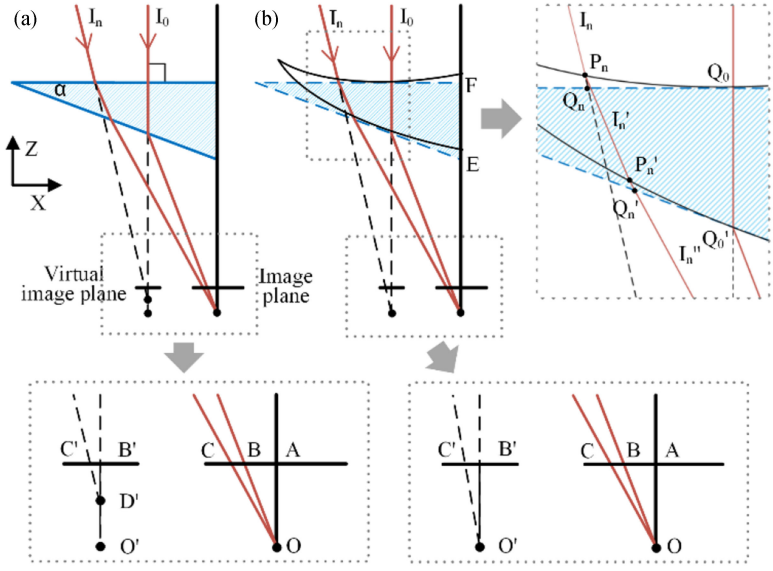

Fig. 3. Ray path of the biprism-based stereovision system: (a) prism with a flat surface; (b) prism with a freeform surface.

Fig. 2(b). In the following section, we will describe the establishment of the constraints for the virtual pinhole camera and how to use them to design the freeform surface of the prism.

2.1. The Constraints of Virtual Pinhole Camera

Because the prism is symmetrical, only light refraction through half of a biprism in the horizontal (O−XZ) plane is used for the detailed illustration. As shown in Fig. 3(a), the actual camera coordinate system is attached to a pinhole camera, whose origin O coincides with the optical center, and a biprism is placed in front of the image plane. AO is the focal length of the real camera. B is the center point of the left half real image plane. I_0 is a ray coming from the point at infinity, which is perpendicular to the bottom surface of the biprism, and its refracted ray projects to point B coincidentally. First, to satisfy the standard epipolar geometry requirement, which indicates that the virtual horizontal image planes must be aligned and the epipolar line should be a horizontal line, the virtual camera is defined based on the following principles: (1) the optical center O' of the virtual camera is located on the extension line of I_0; (2) the focal length of the virtual camera $B'O'$ is identical to that of the real camera; and (3) the virtual image plane is one-half image plane of the

real camera in terms of the shape and size. However, under this condition, for a flat-prism-based stereovision system, the two virtual cameras can hardly satisfy the pinhole model. For example, as shown in Fig. 3(a), if I_n is another ray from a finite object point, its refracted ray projects to point C on the real camera image plane, but the extension line of I_n cannot converge to point O' in most cases. Thus, we must add two other constraints to construct the freeform surfaces, so that it can satisfy the pinhole model. As shown in Fig. 3(b), the center ray I_0 intersects with the two planes of the prism at points Q_0 and Q'_0. If there are two freeform surfaces that are tangent to the two surfaces of the prism at points Q_0 and Q'_0, we assume that: (1) all backward extension lines of the rays that come from O after two refractions converge to point O'; and (2) the distances between points C' and B' are restricted to be identical to the distances between points C and B, so the virtual image sensor has the same pixel size as the real image sensor.

2.2. Design the Freeform Surface of the Prism

Based on the proposed constraints, we can derive the differential equations that can express the refraction process of the freeform prism. To delineate the fundamental of necessary differential equations for the analysis of our design, the differential equation that can represent the ray refraction through an arbitrary curved surface is first provided. We assume that there is a curved surface in three-dimensional Cartesian coordinates, which separates two different media with refractive indices k and k'. $I = [i_x, , i_y, i_z]^T$ is the incident ray; $I' = [i'_x, , i'_y, i'_z]^T$ is the refracted ray; $P = [x, y, z]^T$ is the incident point; T and N are the tangent vector and normal vector of the surface at point P, respectively. If the normal rectilinear congruence of point P is given by $x = x\,(t)$, $y = y\,(t)$ and $z = z(t)$, where t is the parameter of point P, then the differential equation of the refracted rat through an arbitrary curved surface is expressed by:

$$\frac{dz}{dt} = -\frac{\frac{dx}{dt}(ki_x - k'i'_x) + \frac{dy}{dt}(ki_y - k'i'_y)}{(ki_z - k'i'_z)}. \tag{1}$$

In Fig. 3(b), $I_n = [i_{nx}, i_{ny}, i_{nz}]^T$ is the incident ray; $I'_n = [i'_{nx}, i'_{ny}, i'_{nz}]^T$ and $In'' = [inx'', iny'', inz'']T$ are the refracted rays after two refractions by the freeform prism. $P_n = [p_{nx}, p_{ny}, p_{nz}]^T$ and $P'_n = [p'_{nx}, p'_{ny}, p'_{nz}]T$ are the incident points of two refractions of the freeform prism, and $Q_n = [q_{nx}, q_{ny}, q_{nz}]^T$ and $Q'_n = [q'_{nx}, q'_{ny}, q'_{nz}]^T$ are the incident points of twice-refraction of the original flat prism. Assuming that the prism material is optically homogeneous and k' is the refractive index of the medium in the prism, according to Eq. (1), the following equations are obtained:

$$\begin{cases} \frac{dp_{nz}}{dt} = -\frac{\frac{dp_{nx}}{dt}(i_{nx} - k'i'_{nx}) + \frac{dp_{ny}}{dt}(i_{ny} - k'i'_{ny})}{(i_{nz} - k'i_{nz}')} \\ \frac{dp'_{nz}}{dt} = -\frac{\frac{dp'_{nx}}{dt}(k'i'_{nx} - i''_{nx}) + \frac{dp'_{ny}}{dt}(k'i'_{ny} - i''_{ny})}{(k'i'_{nz} - i''_{nz})} \end{cases}. \tag{2}$$

To design a freeform prism, the parameters of an original PbS system must be first provided. Then, the values of I_n, I''_n, Q_n, and Q'_n can be calculated by the coordinates of each offset point (for example, C and C' in Fig. 3(b)). Moreover, according to the equations of the line I_n, and I''_n, p_{nx}, p_{ny}, p'_{nx} and p'_{ny} can be expressed as

$$\begin{cases} p_{nx} = \frac{i_{nx}}{i_{nz}}(p_{nz} - q_{nz}) + q_{nx} \\ p_{ny} = \frac{i_{ny}}{i_{nz}}(p_{nz} - q_{nz}) + q_{ny} \\ p'_{nx} = \frac{i''_{nx}}{i''_{nz}}(p'_{nz} - q'_{nz}) + q'_{nx} \\ p'_{ny} = \frac{i''_{ny}}{i''_{nz}}(p'_{nz} - q'_{nz}) + q'_{ny} \end{cases} \tag{3}$$

If we substitute Eq. (3) into Eq. (2), after some transformations and simplifications, the final differential equations that can be used for iterative computations are:

$$\begin{cases} \frac{dp_{nz}}{dt} = \frac{i_{nz}(i_{nx}-k'i'_{nx})}{k'(l_n\cdot l'_n)-1}\left[\frac{dq_{nx}}{dt}+(p_{nz}-q_{nz})\frac{d\left(\frac{i_{nx}}{i_{nz}}\right)}{dt}\right] \\ \qquad +\frac{i_{nz}(i_{ny}-k'i'_{ny})}{k'(l_n\cdot l'_n)-1}\left[\frac{dq_{ny}}{dt}+(p_{nz}-q_{nz})\frac{d\left(\frac{i_{ny}}{i_{nz}}\right)}{dt}\right] \\ \frac{dp'_{nz}}{dt} = \frac{i''_{nz}(k'i'_{nx}-i''_{nx})}{1-k'(l'_n\cdot l''_n)}\left[\frac{dq'_{nx}}{dt}+(p'_{nz}-q'_{nz})\frac{d\left(\frac{i''_{nx}}{i''_{nz}}\right)}{dt}-\frac{dq'_{nz}}{dt}\frac{i''_{nx}}{i''_{nz}}\right] \\ \qquad +\frac{i''_{nz}(k'i'_{ny}-i''_{ny})}{1-k'(l'_n\cdot l''_n)}\left[\frac{dq'_{ny}}{dt}+(p'_{nz}-q'_{nz})\frac{d\left(\frac{i''_{ny}}{i''_{nz}}\right)}{dt}-\frac{dq'_{nz}}{dt}\frac{i''_{ny}}{i''_{nz}}\right] \end{cases} . \tag{4}$$

In practical applications, all parameters in Eq. (4) are known or can be calculated except p_{nz} and p'_{nz}. Therefore, the only required effort is to solve these first-order ordinary differential equations. If we set the initial iteration point to Q_0 and Q'_0, the numerical solutions of Eq. (4), which expresses the discrete coordinates of the freeform prism surfaces in the Z direction, can be solved by the Runge-Kutta method. Then, the same operation is repeated for subsequent points on the freeform optical surfaces. Moreover, the coordinates of the freeform prism surfaces in the X and Y directions can be easily acquired through the functions of lines l_n and l''_n using the known value of the Z coordinate. In addition, to acquire the entire surface of the freeform prism, the iterations must be performed in four directions (left, right, top and down) from the initial points Q_0 and Q'_0.

We further perform a detailed numerical simulation to test our proposed method. First, the top surface (Fig. 3(a)) of the flat prism is set to be parallel to the plane X-Z, and the resolutions of the camera sensor are set to $1920 * 1080$ in the simulation. Then, the angle of the flat prism can be calculated as followed, so that the refracted ray of I0 can precisely project to the center of the half-image plane.

$$\alpha = \frac{\arctan(\sin(\arctan(s\cdot r/4f)))}{n' - \cos(\arctan(s\cdot r/4f))}, \tag{5}$$

where α is the angle of the prism, s is the pixel size of the real camera, r is the resolution of the camera in the X direction, and f is the focal length of the camera. If the original parameters in this simulation are: $s = 0.0055$ mm, $f = 35$ mm, and $k = 1.48$, then, the angle of the prism can be obtained as $\boldsymbol{\alpha} = 8.85$ degree. In this simulation, the length of the iteration step is selected to be identical to the pixel size of the camera in both X and Y directions. We also set the number of roundtrips to 960 for the left and right iterative directions and 540 for the top and down iterative directions, so that the calculation can cover the entire image plane.

The discrete point cloud of the freeform prism has been calculated with the above parameters. We also implement the surface fitting with the polynomials as follows:

$$z(x, y) = \sum_{m=0}^{p}\sum_{n=0}^{p} C_{(m,n)}x^m y^n, \tag{6}$$

where $1 \le m + n \le p$, $C_{(m,n)}$ is the coefficient. Because the two surfaces are symmetrical with respect to the XOZ plane, only the even terms have been used for calculation. When $p = 5$, the surface profile of the freeform prism is shown in Fig. 4(a).

3. Experiment

To ensure proper convergence of the proposed method, we plot the effect of the step size in the ray tracing computation. The horizontal axis is the step size, which varied from 91 μm to 1 μm. The vertical axis is the average distance error from the optical center of the virtual camera to the intersection points between the reverse extension lines of the refracted ray and the optical axis.

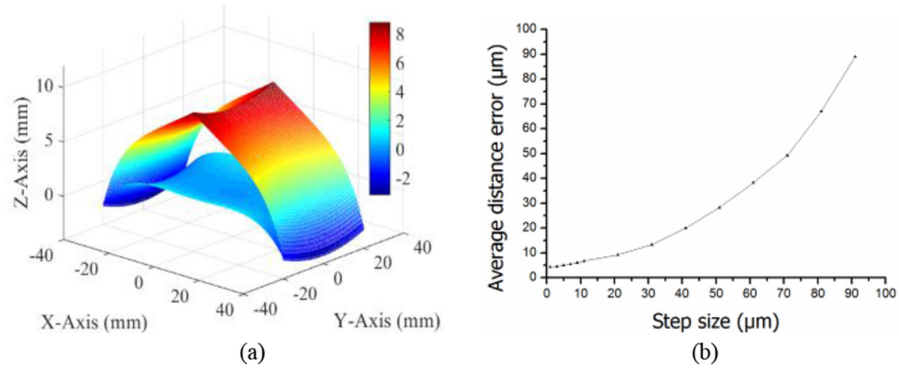

Fig. 4. Calculation results: (a) Fitting surfaces of the freeform prism. (b) Effect of the step size in calculating the freeform surfaces.

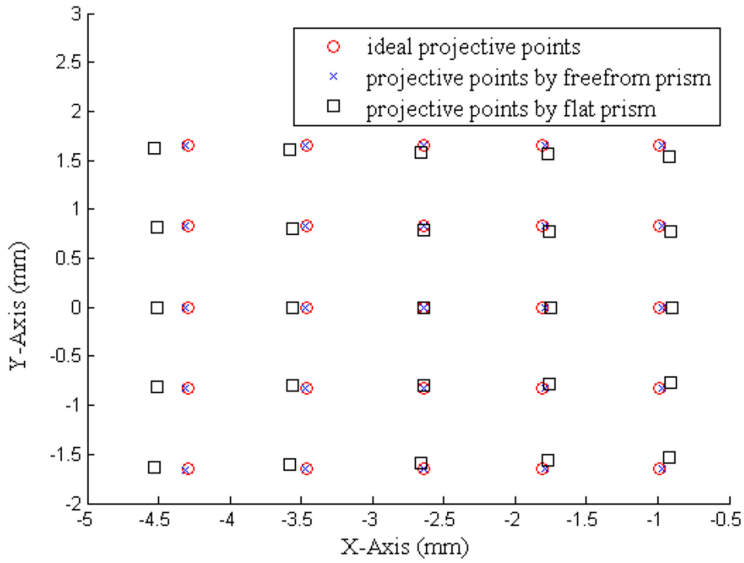

Fig. 5. Comparisons of the reprojection errors.

When the step size decreases, the results will converge to the optical center of the virtual camera, as shown in Fig. 4(b).

Using the calculated surfaces profile, the reprojection error of the virtual camera can be obtained, as shown in Fig. 5. Some image points in the real camera image plane are discretionarily selected, and their light rays from the optical center are refracted by the freeform prism surfaces and back traced to the image plane of the virtual camera. As a comparison, the same operations are implemented for the regular flat prism, whose parameters are set to be equal to the initialization parameter to calculate the freeform prism. Since both freeform prism and flat prism are symmetric with respect to the X-Z plane, only half of the image plane is shown. Table 1 shows the average reprojection errors of the selected points after two refractions by the flat prism and freeform prism. The imaging precision of the vertical direction has been significantly improved by the freeform prism.

We designed a system with the presented method and the described parameters using Zemax. A bilateral telecentric lens is used to evaluate the performance of this method. A monochromatic source with a center wavelength of 486 nm was used in the system. BK7 glass was chosen as the material of the freeform prism, with the refractive index of 1.5168 and the Abbe Number of

TABLE 1
Comparison of the Average Reprojection Errors Between the Flat Prism and the Freeform Prism

	Horizontal error(mm)	Vertical error(mm)	Average error(mm)
Flat prism	0.0604	0.0936	0.0670
Freeform prism	0.0154	0.0011	0.00825

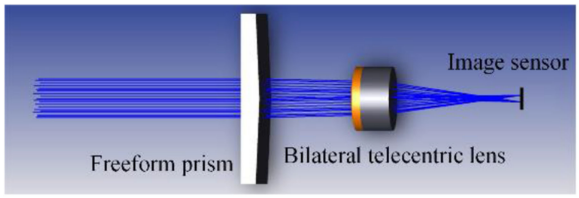

Fig. 6. The structure and optical path of the proposed system.

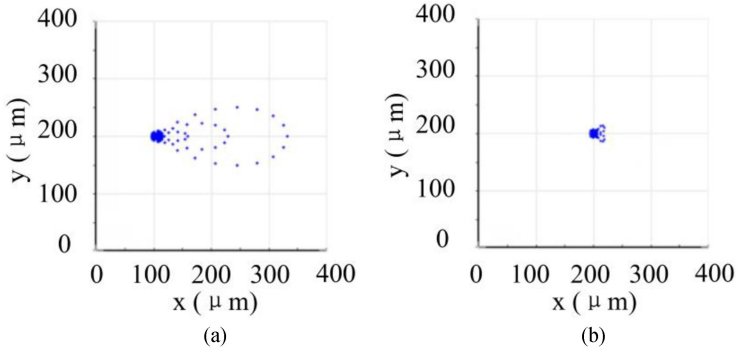

Fig. 7. Spot size. (a) Flat prism, RMS radius is 64.004 μm. (b) Freeform prism, RMS radius is 6.259 μm.

64.167. The field view of the input beam was $\pm$8 degree, and the entrance diameter of the light is 30 mm. The structure and optical path of the Pbs system is shown in Fig. 6, and the magnification of the bilateral telecentric lens was 0.55, and its numerical aperture was 0.09. Fig. 7 and Fig. 8 showed that the performance of freeform prism superior to flat prism in terms of spot size and field curvature.

We used the Optical Transfer Function (OTF) to evaluate the imaging quality of the Pbs system with flat surfaces and the Pbs system with freeform surfaces (results are shown in Fig. 7). The ordinate axis represents the modulus of the OTF (ie, Modulation Transfer Function, MTF). It can be seen from Fig. 7 that the freeform prism is superior to the flat prism in terms of imaging quality in the radial and tangential directions, system astigmatism, contrast characteristics, resolution characteristics, and edge-to-center imaging quality consistency. Figures 1 and 9 show that a better image quality can be expected FOV for the freeform surface compared with flat surface.

We did a tolerance analysis of the system (As shown in Table 2). Spot size is an important indicator for assessing imaging quality, so we used spot size to assess imaging quality in tolerance analysis. We analyzed the imaging quality of the freeform prism system after adding the error value to determine the sensitivity of each surface of the prism to the error. The effect of shape tolerance and position tolerance on imaging quality is thus obtained. It can be seen from the tolerance analysis that the error of the eccentric degree (TEDX 2) of the back surface in the x-axis direction has the greatest influence on the imaging quality. The coaxiality of the x-axis direction between the front and rear surfaces (TEDX 1-2) and the curvature radius of the front surface (TFRN 1) also affect the

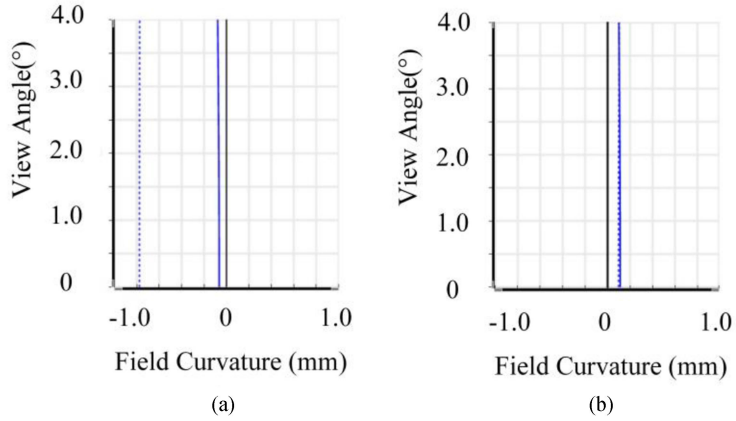

Fig. 8. Field curvature. (a) Flat prism. (b) Freeform prism.

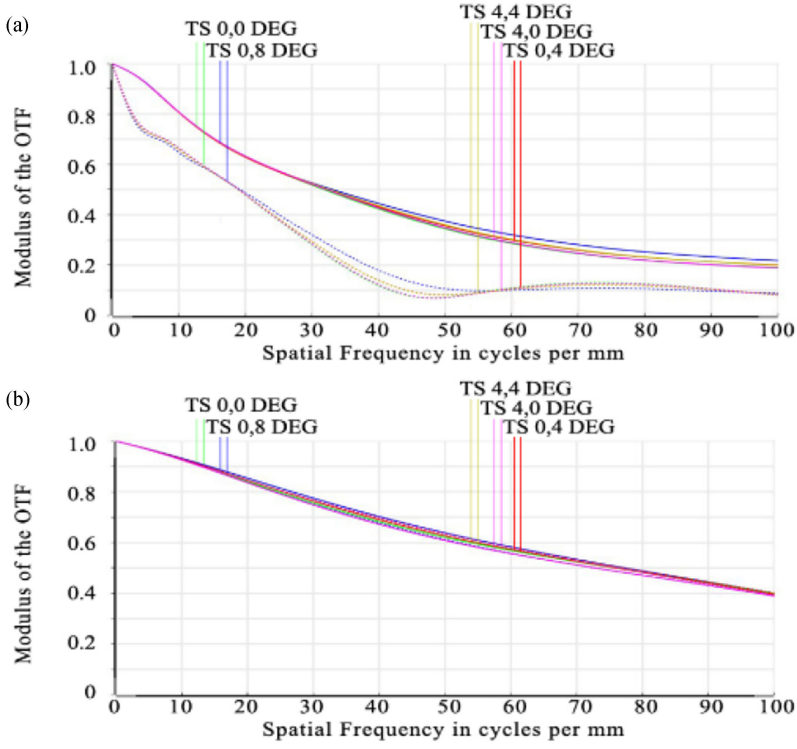

Fig. 9. MTF curves of the system. (a) the PbS system with flat surfaces; (b) the PbS system with freeform surfaces.

imaging quality. However, the parallelism between the front and rear surfaces in the x-axis direction (TETX 1-2), the angle between the front surface and the x-axis (TETX 1), and the angle between the front surface and the y-axis (TETY 1) have little effect on the image quality. So in order to ensure imaging quality, the errors of TEDX 2, TEDX 1-2 and TFRN 1 should be minimized during the processing of freeform prism.

In addition, we have coded a program to implement the freeform prism design algorithm. Then, the users can easily acquire the point cloud and fitting surfaces according to their personal setting of

TABLE 2
Tolerance Analysis

Tolerance type	Surface	Deviation value	Actual spot radius	Spot radius error	Error rate
TFRN	1	1000.00μm	5.33	0.73	16%
TFRN	2	1000.00μm	4.74	0.14	3%
TTHI	1-2	200.00μm	4.71	0.11	2%
TEDX	1-2	200.00μm	6.26	1.66	36%
TEDY	1-2	200.00μm	4.65	0.05	1%
TETX	1-2	0.2°	4.60	0.00	0%
TETY	1-2	0.2°	4.71	0.11	2%
TETY	1	0.2°	4.60	0.00	0%
TETX	1	0.2°	4.60	0.00	0%
TEDX	2	200.00μm	7.04	2.44	53%
TEDY	2	200.00μm	4.76	0.17	4%

Note: The ideal spot radius is 4.60 μm; **TFRN:** Curvature radius of the surface; **TTHI:** Thickness between surfaces; **TEDX:** Eccentric distance of the surface in the x-axis direction; **TEDY:** Eccentric distance of the surface in the y-axis direction; **TETX:** The angle between the surface and the x-axis; **TETY:** The angle between the surface and the y-axis; **Surface 1:** The front surface; **Surface 2:** The rear surface; **Surface 1-2:** between the front and rear surface.

camera parameters and they do not need the freeform prism whereas different views as interactive operation, as we show in Code 1 (Ref. [22]).

4. Conclusion

In conclusion, we have presented a freeform prism design method to achieve the three-dimensional stereo imaging capability for machine vision applications. To improve the spatial resolution in z direction, all refracting surfaces of the prism are designed to freeform feature. The results show that our method can compensate the image distortion of the flat prism and reduce the projection error to the pixel level. And freeform prism offers significant advantages over flat prism in space-constrained, high-precision and highly dynamic 3D measurements. Compared with the image-based method, the freeform prism method has completed image correction before the image is captured by the image sensor, which greatly improves the real-time performance of the system and does not require additional hardware computing resources. In addition, the method can be extended to multi-ocular, freeform, prism-based stereovision systems.

References

[1] S.-P. Yang, J.-J. Kim, K.-W. Jang, W.-K. Song, and K.-H. Jeong, "Compact stereo endoscopic camera using microprism arrays," *Opt. Lett.*, vol. 41, no. 6, pp. 1285–1288, 2016.
[2] X. Y. Cui, Y. Q. Tong, and R. Jing, "Using a bi-prism endoscopic system for three-dimensional measurement," *J. Med. Imag. Health Inform.*, vol. 6, no. 5, pp. 1293–1297, 2016.
[3] L. Li and A. Y. Yi, "Design and fabrication of a freeform prism array for 3D microscopy," *J. Opt. Soc. Amer. A*, vol. 27, no. 12, pp. 2613–2620, 2010.
[4] L. F. Wu, J. G. Zhu, H. M. Xie, and Q. Zhang, "An accurate method for shape retrieval and displacement measurement using bi-prism-based single lens 3D digital image correlation," *Exp. Mech.*, vol. 56, no. 9, pp. 1611–1624, 2016.

[5] Q. Gao, H. Wang, and J. Wang, "A single camera volumetric particle image velocimetry and its application," *Sci. China Technol. Sci.*, vol. 55, no. 9, pp. 2501–2510, 2012.
[6] M. Zhang, Y. Piao, J.-J. Lee, D. Shin, and B.-G. Lee, "Visualization of partially occluded 3D object using wedge prism-based axially distributed sensing," *Opt. Commun.*, vol. 313, pp. 204–209, 2014.
[7] D. H. Lee and I. Kweon, "A novel stereo camera system by a biprism," *IEEE Trans. Robot. Autom.*, vol. 16, no. 5, pp. 528–541, Oct. 2000.
[8] K. B. Lim and Y. Xiao, "Virtual stereovision system: New understanding on single-lens stereovision using a biprism," *J. Electron. Imag.*, vol. 14, pp. 41–52, 2005.
[9] D. Wang, K. Bin Lim, and W. L. Kee, "Geometrical approach for rectification of single-lens stereovision system with a triprism," *Mach. Vision Appl.*, vol. 24, no. 4, pp. 821–833, 2013.
[10] K. Bin Lim, W. L. Kee, and D. Wang, "Virtual camera calibration and stereo correspondence of single-lens bi-prism stereovision system using geometrical approach," *Signal Process. Image Commun.*, vol. 28, no. 9, pp. 1059–1071, 2013.
[11] Y. Xiao and K. Bin Lim, "A prism-based single-lens stereovision system: From trinocular to multi-ocular," *Image Vision Comput.*, vol. 25, no. 11, pp. 1725–1736, 2007.
[12] C.-Y. Chen, T.-T. Yang, and W.-S. Sun, "Optics system design applying a micro-prism array of a single lens stereo image pair," *Opt. Exp.*, vol. 16, no. 20, pp. 15495–15505, 2008.
[13] C.-Y. Chen, Q.-L. Deng, W.-S. Sun, Q.-Y. Cheng, B.-S. Lin, and C.-L. Su, "Panoramic stereo photography based on single-lens with a double-symmetric prism," *Opt. Exp.*, vol. 21, no. 7, pp. 8474–8482, 2013.
[14] X. Cui, K. Bin Lim, Q. Guo, and D. Wang, "Accurate geometrical optics model for single-lens stereovision system using a prism," *J. Opt. Soc. Amer. A*, vol. 29, no. 9, pp. 1828–1837, 2012.
[15] X. Cui, K. Bin Lim, Y. Zhao, and W. L. Kee, "Single-lens stereovision system using a prism: Position estimation of a multi-ocular prism," *J. Opt. Soc. Amer. A*, vol. 31, no. 5, pp. 1074–1082, 2014.
[16] X. Cui, Y. Zhao, K. Lim, and T. Wu, "Perspective projection model for prism-based stereovision," *Opt. Exp.*, vol. 23, no. 21, pp. 27542–27557, 2015.
[17] L. Wu, J. Zhu, and H. Xie, "A modified virtual point model of the 3D DIC technique using a single camera and a bi-prism," *Meas. Sci. Technol.*, vol. 25, no. 11, 2014, Art. no. 115008.
[18] L. Wu, J. Zhu, and H. Xie, "Single-lens 3D digital image correlation system based on a bilateral telecentric lens and a bi-prism: Validation and application," *Appl. Opt.*, vol. 54, no. 26, pp. 7842–7850, 2015.
[19] K. Bin Lim and B. Qian, "Biprism distortion modeling and calibration for a single-lens stereovision system," *J. Opt. Soc. Amer. A*, vol. 33, no. 11, pp. 2213–2224, 2016.
[20] K. Genovese, L. Casaletto, J. A. Rayas, V. Flores, and A. Martinez, "Stereo-digital image correlation (DIC) measurements with a single camera using a biprism," *Opt. Lasers Eng.*, vol. 51, no. 3, pp. 278–285, 2013.
[21] Y. Maeda, D. Miyazaki, and T. Mukai, "Volumetric display using a rotating prism sheet as an optical image scanner," *Appl. Opt.*, vol. 52, no. 1, pp. A182–A187, 2013.
[22] X. Y. Cui, "Freeform prism design demo," Github, 2019. [Online]. Available: https://github.com/wangliqianNEU/Freeform-prism-design-DEMO